ELSEVIER

Contents lists available at ScienceDirect

Chemical Engineering Journal

journal homepage: www.elsevier.com/locate/cej



A self-healing coating containing curcumin for osteoimmunomodulation to ameliorate osseointegration



Bo Li^{a,e,1}, Run Huang^{b,1}, Jing Ye^{a,1}, Lei Liu^b, Liang Qin^b, Jianhong Zhou^f, Yufeng Zheng^c, Shuilin Wu^d, Yong Han^{a,*}

- ^a State Key Laboratory for Mechanical Behavior of Materials, Xi'an Jiaotong University, Xi'an 710049, China
- School of Materials Science and Engineering, Anhui University of Science and Technology, Huainan, 232001, China
- Center for Biomedical Materials and Tissue Engineering, Academy for Advanced Interdisciplinary Studies, Peking University, Beijing 100871, China
- ^d School of Materials Science & Engineering, the Key Laboratory of Advanced Ceramics and Machining Technology by the Ministry of Education of China, Tianjin University, Tianjin 300072, China
- e School of Life Science and Technology, Xi'an Jiaotong University, Xi'an 710049, China
- ^f Institute of Physics & Optoeletronics Technology, Baoji University of Arts and Science, Baoji 721016, China

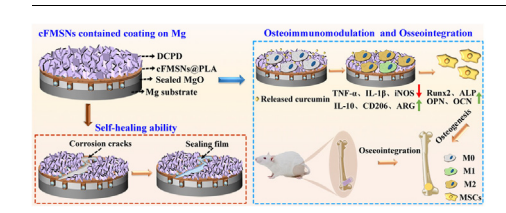
HIGHLIGHTS

- A new coating with self-healing and osteoimmunomodulatory effects was formed on Mg.
- FMSN in the coating functioned as corrosion inhibitor and nanocontainer of curcumin.
- The coating exhibited self-healing ability to provide long-term protection to Mg.
- The coating polarized the macrophage into M2 phenotype to enhance osseointegration.

ARTICLE INFO

Keywords:
Magnesium
Self-healing coating
Controllable release
Osteoimmunomodulation
Osseointegration

GRAPHICAL ABSTRACT



ABSTRACT

To enhance corrosion resistance and osseointegration of Mg-based endosseous implants, novel coatings with selfhealing and osteoimmunomodulation functions were fabricated on Mg. The coatings exhibited similar threelayered structure, comprising an inner layer of MgO, an interlayer of poly-L-lactide containing curcumin loaded F-encapsulated mesoporous silica nanocontainers (cFMSNs) and an outer layer of dicalcium phosphate dehydrate, while the amounts of cFMSNs contained in the interlayers were different (thus namely 5FMSN, 10FMSN, 20FMSN). Localized-electrochemical impedance spectroscopy, electrochemical and immersion tests were used to investigate self-healing property and corrosion resistance of the coatings, moreover, curcumin release, immunomodulation effects and osseointegration of these coatings were also assayed, together with cFMSNs-free coating (0FMSN). Due to the cFMSNs functioning as corrosion inhibitor, cFMSNs-contained coatings exhibited obvious self-healing property to enhance protection to Mg in vitro and in vivo compared to 0FMSN, and the enhancements were more pronounced with cFMSNs increase. cFMSNs-contained coatings sustainably released curcumin, and the accumulative curcumin concentration of the 20FMSN immersed physiological saline (PS) was $1.51~\mu M$ after 10 days of immersion, which was higher than those of the PS immersing 10FMSN ($1.02~\mu M$) and 5FMSN (0.31 μM). Owing to the released curcumin, cFMSNs-contained coatings significantly modulated the immune microenvironment towards favoring osteo-differentiation and extracellular matrix mineralization of bone marrow stem cells, consequently exhibited better osseointegration compared to 0FMSN. 20FMSN exhibited

E-mail address: yonghan@mail.xjtu.edu.cn (Y. Han).

^{*} Corresponding author.

¹ Co-first authors: These authors contributed equally to this work.

higher immunomodulatory efficiency compared to 10FMSN and 5FMSN, and thus achieved the best osseointegration *in vivo*. Our work paves an alternative way to design coatings on Mg for realizing improved clinical performance.

1. Introduction

Magnesium and its alloys rise great potential as temporary endosseous implants attributing to their relative high mechanical strength, elastic modulus similar with that of natural bone, and biodegradability in physiological environment without toxicity. Unfortunately, high degradation rate limits their clinical application [1]. To overcome the demerit, many approaches has been tried, where surface modification-

derived coatings exhibited effective protection to Mg substrates against corrosion *in vitro* and *in vivo* [2], such as zoledronic-acid-loaded PLA/brushite coating [3], chitosan coating [4], Ca, Sr/P loaded silk fibroin film [5], hydroxyapatite/MgO coating [6,7]. Among these coatings, micro-arc oxidization (MAO)-derived MgO coating exhibited significantly higher protective efficacy [2]. However, the MAOed coatings are inherently porous, weakening their corrosion resistance [8,9]. Therefore, biodegradable, biocompatible and drug-loading available

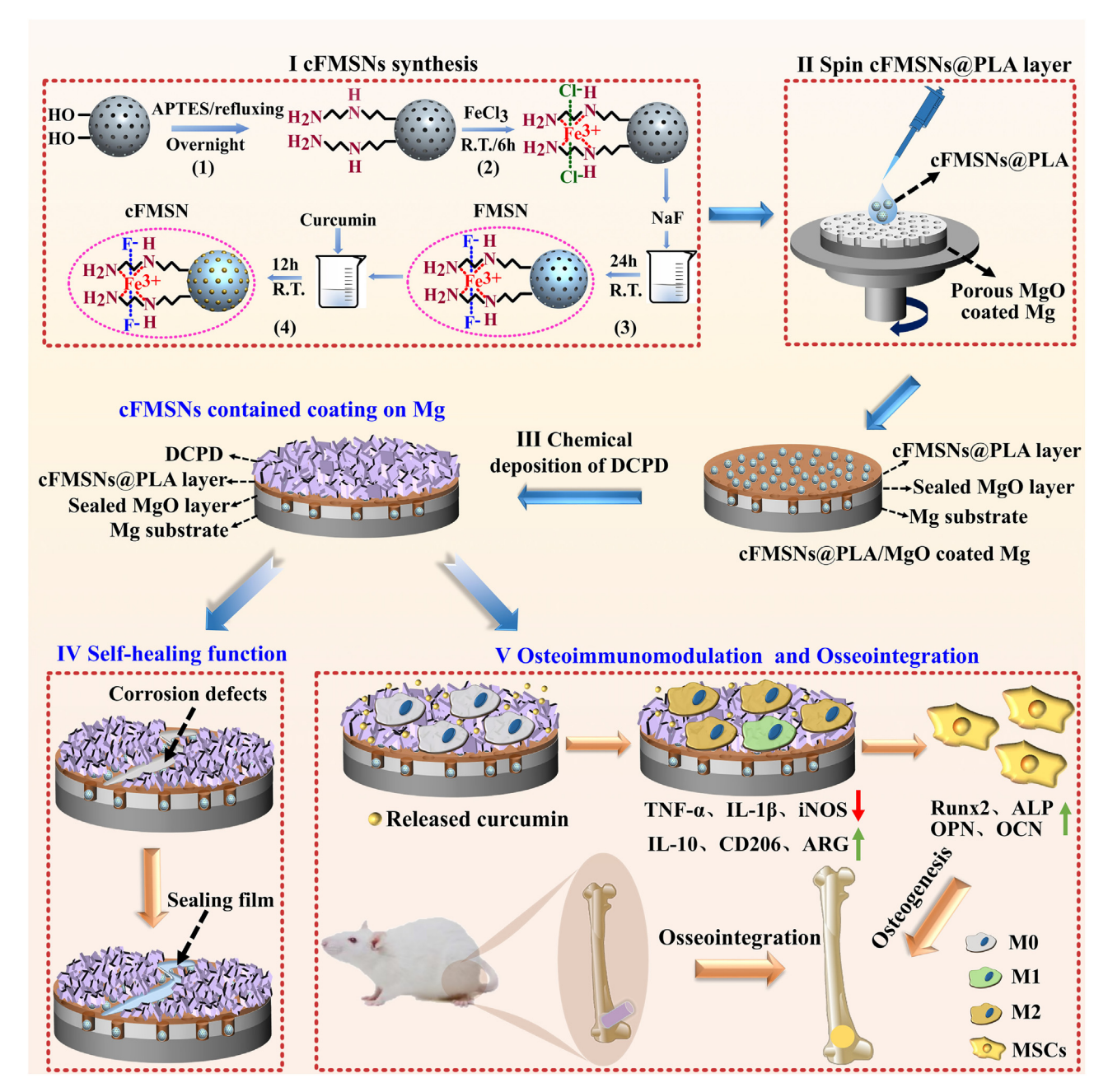


Fig. 1. Schematic representation of the fabrication process of the cFMSNs-contained coating on Mg. (I) cFMSNs synthesis including (1) amino group grafting on MSNs to form chemical active sites, (2) immobilization of Cl ions, (3) F ions encapsulation and (4) curcumin loading (R. T.: room temperature); (II) spin the PLA solution containing cFMSNs on the inner layer of porous MgO to form the interlayer of cFMSNs@PLA; (III) chemical deposition to form the outer layer of DCPD; evaluation of (IV) self-healing as well as (V) osteoimmunomodulation and osseointegration functions of the cFMSNs-contained coatings *in vitro* and *in vivo*.

organic sealants [10], including poly-L-lactide (PLA) [11], chitosan (CS) [12], polycaprolactone (PCL) [13], were used to seal the pores contained in the MAOed coatings. PLA was more acceptable, because its degradation generates acidic intermediate products to neutralize Mgdegradation derived alkalization, moreover, the final degradation products of PLA are water and carbon dioxide without toxicity [11]. Unfortunately, the pore-sealed MAOed coatings would lose their effective protection during long-term immersion, ascribing to the formation of micro-cracks/pores in the coatings [9]. For instance, PLA-sealed MAOed coating exhibited severe corrosion pits on its surface after immersing in Hanks' balanced salt solution for 140 h [11]; organic reagents sealed MAOed coating showed two-orders decrease in impendence after 408 h of immersion in 3.5% NaCl [8]. To further enhance the corrosion resistance of the coatings, corrosion inhibitors (CIs) were loaded in the coatings for achieving the self-healing function. Once physiological fluids penetration-derived microdefects appeared in the coating, the released CIs would react with degradation-derived Mg²⁺ or OH⁻ to form a passive layer and seal the microdefects, achieving the self-healing process and recovering protective efficacy of the coating [14]. Typically, the currently developed self-healing coatings on Mg alloys were Ce²⁺ contained CS/MgO composite coating [15], PO₄³⁻ contained silk fibroin coating [16], and silk-phytic acid (PA)/silk fibroin multilayered coating [16]. However, the CIs contained in these coatings would form insoluble passive layer, such as cerium oxides/hydroxides, which could induce toxicity to hemostatic system and osteolysis [17,18], moreover, the CIs contained in the aforementioned coatings achieved only single function. Alternatively, fluoride (F⁻) encapsulated mesoporous silica nanocontainers (FMSNs) could be served as a CI, employing the released F reacting with Mg²⁺ to form the protective MgF₂ film at micro-defects [19]. More importantly, MgF₂ could be degraded by the Cl⁻-contained body fluids [20] without remaining insoluble nanoparticles or fragments [18]. Furthermore, FMSNs also could be served as nanovehicles to controllably deliver drugs due to their high surface area with good degree of drug loading

Osteogenesis is another major concern for Mg-based endosseous implants, which is divided into distance osteogenesis and contact osteogenesis, the latter is crucial for osseointegration [23]. Contact osteogenesis starts with macrophage-mediated inflammatory response. After implantation, macrophages, revealing two polarized phenotypes of M1 and M2, are recruited to the implant surface to initiate inflammation [24,25]. M1 macrophages destruct the adjacent bone and form fibrous tissues by secreting pro-inflammatory cytokines such as interleukin (IL)-1β, inducible nitric oxide synthase (iNOS), and tumor necrosis factor (TNF)-a. However, M2 macrophages can alleviate inflammation by producing anti-inflammatory cytokines such as IL-10, arginase-1 (ARG) and cluster of differentiation 206 (CD206) and promote bone regeneration by secreting growth factors to support migration, homing and osteo-differentiation of bone marrow stem cells (BMSCs) [24,26,27]. To quickly switch the phenotype of macrophages from M1 to M2, i.e., realize osteoimmunomodulation towards favoring osseointegration, chemical agents and immunomodulatory drugs [28] were immobilized on the surfaces of endosseous implants. Among them, curcumin was received much concern, due to its biosafety, high tolerability [29,30] and versatility [31,32]. For instance, curcumin inhibited Toll-like receptor 4 (TLR4)-mediated signaling pathway and consequently suppressed macrophage polarizing towards M1, reducing the risk of chronic inflammation induced fibrotic encapsulation [24,29,31]. Moreover, curcumin alleviated the receptor activator of nuclear factorκB ligand (RANKL)-induced osteoclast resorption [33,34] and enhanced osteo-differentiation of stem cells through activating phosphatidylinositol-3-kinase (PI3K)/protein kinase B (AKT)/nuclear factor erythroid 2-related factor (Nrf2) signaling pathway [35]. Unfortunately, due to the low solubility and weak chemical stability [31], curcumin should to be loaded in drug-delivery system to keep long term release. As an option, FMSNs, which was chosen for CI, could also be employed to load curcumin. Thus, it can be deduced that loading curcumin-contained FMSNs (cFMSNs) into a coating would simultaneously endow the coating with self-healing and osteoimmunomodulation functions. However, to our best of knowledge, cFMSNs contained coating on Mg with the aforementioned dual-function has not been reported yet. Following osteoimmunomodulation, the recruitment of osteogenesis-related cells to the implant surface, differentiation, and extracellular matrix (ECM) mineralization of the cells occur sequentially to induce contact osteogenesis [36,37], and the osteogenic functions of the cells could be significantly enhanced by Ca-P contained surfaces [38].

Herein, we fabricated a novel coating on Mg, which simultaneously exhibited self-healing and osteoimmunomodulation functions to enhance corrosion resistance and osseointegration of Mg-based implants. The obtained coating composed of dicalcium phosphate dehydrate (DCPD) as an outer layer, PLA containing cFMSNs as an interlayer and pores-sealed MgO with PLA containing cFMSNs as an inner layer. The self-healing property of the coatings with different cFMSNs-loading amounts were tested *in vitro*, and the osteoimmunomodulation and osseointegration of the coatings were evaluated *in vitro* and *in vivo*. Notably, curcumin in the present work is a model drug and can be replaced by other bio-regents to achieve various functions. Thus, the present work provided a new and simple strategy for designing multifunctional coatings with high corrosion resistance on Mg-based endosseous implants.

2. Materials and methods

The entire experimental protocols were schematized in Fig. 1.

2.1. Materials and reagents

WE43 Mg alloy was purchased from Northwest Institute for Nonferrous Metal Research; Cetyltrimethylammonium bromide (CTAB), tetraethoxysila (TEOS), thyl acetate (EA), (3-Aminopropyl) triethoxysilane (APTES), curcumin powder, glutaraldehyde and Alizarin Red were purchased from Sigma-Aldrich Co. Ltd. (USA); PLA powder, 1-propanol, 2-propanol, anhydrous toluene, HCl, FeCl₃, NaF, ethanol, Na₃PO₄, Ca(OH)₂, NaOH, chloroform, Ca(H₂PO₄)₂·H₂O and cetylpyridinum chloride were obtained from Sinopharm Chemical Rengent Co., Ltd. (Shanghai, China); Dulbecco's modified Eagle medium (DMEM)-F12k 1: 1 and antibiotics were purchased from Hyclone Co. Ltd. (USA); fetal bovine serum (FBS, FND500) was purchased from ExCell Bio Co. Ltd. (Shanghai, China); alamarBlue™, Live/ dead staining kit, TRizol reagent and BCA protein assay kits were purchased from Thermo Fisher Scientific Co. Ltd. (USA); First Strand cDNA Synthesis Kit was obtained from Roche Co. Ltd. (Switzerland); BCIP/NBT ALP color development kit was purchased from Beyotime Co. Ltd. (Shanghai, China); SensoLyte® pNPP Alkaline Phosphatase Assay Kit was obtained from AnaSpec Inc. (USA).

2.2. Coating preparation

2.2.1. Synthesis of FMSNs and loading curcumin in the FMSNs

The procedure of FMSNs synthesis was described in previous study [19]. Briefly, 1.0 g CTAB was added into 480 mL deionized water, followed by adding 3.5 mL NaOH solution (2.0 M), and adjusting the temperature of the mixture to 70 °C. After intensely stirring for 30 min, 5.5 mL TEOS and 5.0 mL EA were sequentially added into the mixture under vigorous magnetic stirring to form white precipitate. The precipitation was filtered, washed, and dried overnight at 60 °C. The resultant MSNs were then refluxed in 340 mL 2-propanol containing 10 vol% HCl for 2 h to remove the unreacted CTAB. Then the obtained MSNs were suspended in 120 mL anhydrous toluene under $\rm N_2$ atmosphere. After dropwise adding 3.0 mL APTES, the reactants were stirred and refluxed overnight in $\rm N_2$ ambient. The precipitation was filtered and washed, and then suspended in 140 mL 1-propanol solution with

addition of $1.40~g~FeCl_3$ for 6~h followed by filtrating and washing with water and ethanol. The obtained powder was transferred into 150~mL aqueous solution containing 1.0~g~NaF, followed by stirring for 1~day and washing with ethanol, centrifuging and drying to achieve the synthesis of FMSNs.

Subsequently, 0.1 g of the obtained FMSNs were dispersed in 500 mL ethanol containing 0.5 g curcumin followed by stirring for 12 h in dark at room temperature. Then the mixture was centrifuged, washed and dried to get the cFMSNs.

2.2.2. Micro-arc oxidation

Disc- and pillar-shaped WE43 Mg alloy with the respective size of $\Phi14\times4$ mm, $\Phi1.6\times4$ mm were used as the anodes and stainless steel plate was used as the cathode in an aqueous electrolyte containing 0.02 M Na₃PO₄, 0.135 M Ca(OH)₂, and 0.125 M NaOH to receive MAO. The MAO process lasts for 10 min at 450 V positive pulse voltage, 100 Hz pulse frequency, and 26% duty ratio at a home-made power supply. The obtained coating was named as MAO₀.

2.2.3. DCPD/cFMSNs@PLA layers formed on MAO₀

The preparation of the DCPD/cFMSNs@PLA layer formed on MAO₀ was carried out as follows: the powder of PLA was dissolved in chloroform with 3 wt/v%, then cFMSNs were added into the PLA solution with the concentration of 5, 10, 20 wt% relative to the content of PLA, respectively. 50 μ L PLA solution without or with different cFMSNs concentrations was spin coated on each of MAO₀-coated Mg followed by another 2 times of repetition. The obtained coated Mg were vertically immersed in a supersaturated solution of Ca(H₂PO₄)₂·H₂O with an initial pH of 4.0 overnight at room temperature to deposit DCPD. The resultant coatings were termed as 0FMSN, 5FMSN, 10FMSN, 20FMSN, respectively. The aforementioned procedures were performed in dark.

2.3. Characterizing the structures of the nanospheres and the coatings

The morphologies of MSNs, FMSNs and the constructed coatings were characterized by a field-emission scanning electron microscope (FE-SEM, FEI QUANTA 600F, USA) with an energy-dispersive X-ray spectrometer (EDX). The chemical species of MSNs and FMSNs were examined with X-ray photoelectron spectroscope (XPS; Axis Ultra, U. K.). In XPS tests, Mg K α radiation was used as X-ray source, and the photoelectron take off angle was set at 45°. The obtained XPS spectra were calibrated to C 1s (hydrocarbon C–C, C–H) contribution at the binding energy of 284.8 eV. Transmission electron microscope (TEM; JEOL JEM-2000FX, Japan) operating at 200 kV was used to examine the microstructures of MSNs and FMSNs. Phase compositions of MSNs and FMSNs were examined by an X-ray diffractometer (XRD; X'Pert PRO, Netherlands) with small-angle X-rays scattering mode (SAXS), and the XRD was also used to identify the phase compositions of the constructed coatings over a 20 angle of 20–50° at a step of 0.02°.

2.4. Self-healing ability and corrosion resistance of the coatings

2.4.1. Immersion tests

The immersion tests of the 0FMSN-, 5FMSN-, 10FMSN- and 20FMSN-coated Mg discs were carried out in physiological saline (PS, i.e., 0.9 wt% NaCl aqueous solution) at 37 °C for 21 days, together with the bare Mg disc. Each of the discs was sealed with epoxy resin in order to expose only one side to the solution. The hydrogen evolution and pH value of each disc immersed PS were monitored. After 3 days of immersion, Mg²⁺ and Ca²⁺ concentrations of each disc immersed solution were examined with inductively coupled plasma atomic emission spectrometry (ICP-AES; PerkinElmer, NexION 350D, USA). All tested values were averaged from three specimens at each immersion time point. After 21 days of immersion, the immersed discs were taken out of the PS prior to the washing with deionized water and drying, the surface macro-morphologies of the discs were captured using a digital

camera (Canon, Japan).

2.4.2. Electrochemical tests

Potentiodynamic polarization (PDP) and electrochemical impedance spectroscopy (EIS) tests of the coated Mg and bare Mg discs were performed before and after 24 h of immersion in PS, using an autolab potentiostat set (PGSTAT, 128 N, Metrohm). For PDP tests, each of the discs was immersed in a three electrode cell containing PS solution to act as a working electrode. A saturated calomel electrode (SCE) was used as the reference electrode and Pt as the auxiliary electrode. The PDP curves were measured from $-1.5~\rm V$ to $0.5~\rm V$ (referred to the SCE) at a scanning rate of 5 mV/s. The EIS tests were carried out at the open circuit potential, and a 10 mV amplitude sine wave was applied throughout the experiments at frequencies between $1\times10^{-1}~\rm Hz$ and $1\times10^{5}~\rm Hz$. The impedance data were analyzed using the Zview 3.1 software (USA). All PDP and EIS tests for the bare Mg disc and each kind of the coated discs were performed in triplicate.

2.4.3. Localized electrochemical impedance spectroscopy (LEIS) measurements

Self-healing property of the coatings were tested using LEIS as previously described [39]. Briefly, each of the coated discs was sealed with epoxy resin leaving only one side. An artificial defect (0.5 mm \times 1 mm) exposing the substrate was produced on the surface of each coated disc using a diamond cone, and then the coated disc with artificial defect was immersed in PS for 24 h. Subsequently, a five-electrode configuration (VersaSCAN, USA) was used to obtain the impedance values via LEIS probe scanning over a 2.0 mm \times 3.0 mm sized area including the artificial defect on the coated disc in PS and a frequency of 10 Hz was used during LEIS scanning. Each type of the coated discs was tested in triplicate.

2.4.4. Curcumin released from the coated Mg in vitro

The assay of curcumin released from the 5FMSN-, 10FMSN- and 20FMSN-coated Mg discs was carried out in PS (pH 7.4) at 37 °C for 10 days. To exclude the interference from other elements derived from coating degradation, 0FMSN-coated disc, defined as a blank group, was also immersed in PS along with other groups. The coated discs were placed in 24-well plates and immersed in 1 mL PS. At each time point, the PS were pipetted and transferred into cuvettes, followed by adding fresh PS into each well. The absorbance of the solution in cuvette was measured by a Multiscan GO microreader (Thermo Scientific, USA) at 425 nm, and then the absorbance of the blank groups was deducted from those of experimental groups. The concentrations of curcumin were drawn from a standard curve of absorbance *versus* known standards of curcumin concentrations. For each type of the coated discs, four specimens were tested.

2.5. Assessment of macrophages polarization and osteogenetic functions of BMSCs in vitro

2.5.1. Cell culture

Mouse macrophage, Raw264.7, and BMSCs were purchased from the Institute of Biochemistry and Cell Biology of Chinese Academy of Sciences (Shanghai, China). Both the macrophages and BMSCs were incubated with the culture medium, containing DMEM-F12k 1: 1 with 10% FBS and 1% antibiotics and in a humidified atmosphere incubator with 5% $\rm CO_2$ and 95% air at 37 °C. And the culture medium used for both cells were refreshed every 2 days throughout the whole incubation period.

2.5.2. Macrophages polarization on the coated discs

Alamar blue assay and live/dead staining were performed to identify the cytocompatibilities of the coated Mg discs. Briefly, the 0FMSN-, 5FMSN-, 10FMSN- and 20FMSN-coated Mg discs were placed centrally in 24-well plates. RAW264.7 were seeded on the discs with a density of

 1×10^4 cells per well and incubated for 1, 3, and 5 days. At each time point, the culture medium was discarded, followed by rinsing each of the cell-adhered coated discs with phosphate buffer saline (PBS) twice and transferring to new 24-well plates. 500 μL culture medium containing 10 vol% alamarBlue^TM was added to each well and incubated for 4 h. 100 μL of the resultant solution was transferred to new 96-well plates followed by measuring the absorbance at 570 nm and 600 nm using Multiscan GO microreader (Thermo Scientific, USA). The values of OD_{570nm}/OD_{600nm} were used to reveal the mitochondrial activities of the macrophages cultured on the coatings. Four specimens from each group were tested, and each test was repeated four times.

Live/dead staining kit was conducted to identify the viable Raw264.7 cells on the coated Mg after 1, 3, and 5 days of incubation. At each time point, the cell-adhered coated discs were washed with PBS followed by adding 300 μL of PBS containing ethidium-homodimer-1 (4 μM) and calcein-AM (2 μM) to each well and incubating at 37 °C for 30 min. The fluorescence-stained cells were analyzed using a fluorescence microscope (Nikon, Japan).

After 1, 3 and 5 days of incubation, the cell-adhered samples were washed with PBS and fixed with 4% glutaraldehyde for 1 h at 4 $^{\circ}$ C. The cell-adhered coated discs were then dehydrated in gradient ethanol, followed by vacuum drying. After coating gold, the cell-adhered coated discs were observed under FE-SEM for cell morphologies.

The expressions of inflammation-related genes of the macrophages, cultured on the coated discs for 3 and 5 days, were evaluated with real time polymerase chain reaction (RT-PCR). The total RNA was isolated using the TRizol reagent and reversed transcribed into complementary DNA using First Strand cDNA Synthesis Kit. Expressions of M1 phenotype markers, including TNF- α , IL-1 β , iNOS and M2 phenotype markers, including IL-10, CD206, and ARG were quantified using detection system (LightCycler@96, Roche, Switzerland). Data analysis was carried out using LightCycler@96 instrument software 1.1 (Roche, Switzerland). The housekeeping gene, glyceraldehyde-3-phosphate dehydro-genase (GAPDH), was used as an endogenous reference gene to normalize calculation through the $2^{-\Delta\Delta Ct}$ method. The sequences of the specific primer for these genes were listed in Table S1. Four samples from each group were tested at each time point, and the tests were independently repeated four times.

2.5.3. Osteogenetic modulation of the coatings

The RAW264.7 cells were seeded on the 0FMSN-, 5FMSN-, 10FMSN- and 20FMSN-coated Mg discs as described in Section 2.5.2, and the culture medium after incubating the cells seeded on the coated discs for 3 days were collected and centrifuged to get the supernatants. The obtained supernatants, termed as conditioned culture medium (CCM), were kept at 4 °C until use. BMSCs were seeded in 48-well plates with a density of 5×10^3 cells for each well and cultured for 24 h to allow the cells adhering to the plate. Thereafter, the culture medium was replaced by CCM and refreshed every 2 days. After 7 and 14 days of incubation, the osteogenesis-related gene expressions including runt-related transcription factor 2 (Runx2), Alkaline phosphatase (ALP), osteopontin (OPN) and osteocalcin (OCN) were tested by RT-PCR using the method described in Section 2.5.2. For each kind of CCM, cells obtained from three replicated wells were tested at each time point, and the tests were independently repeated four times.

After culturing with CCM for 7 days, the BMSCs adhered on the culture plates were washed with PBS and fixed with 4% glutaraldehyde for 1 h. ALP staining assay was conducted with the BCIP/NBT ALP color development kit follow the manufacturer's instruction. In parallel, ALP activities of the BMSCs was determined through SensoLyte® pNPP Alkaline Phosphatase Assay Kit. Briefly, the BMSCs were lysed with the lysis solution contained in the assay kit at 4 °C for 10 min followed by centrifuging to get the supernatants. The obtained supernatants were transferred to new 96-well plates prior to the addition of p-nitrophenyl phosphate (p-NPP) substrates and incubated at 37 °C for 30 min. The absorbance was measured by a Multiscan GO microreader (Thermo

Scientific, USA) at 405 nm and the ALP activities were drawn from a standard curve of absorbance *versus* known standards of ALP activities, and the standard samples were tested in parallel with the experimental supernatants. The results were normalized to the intracellular total protein contents tested by BCA protein assay kits. Triplicate wells containing cells from each type of CCM treatment group were tested at each incubation time point, and the tests were independently repeated four times.

ECM mineralization of BMSCs was analyzed using Alizarin Red staining. The BMSCs were incubated in CCM for 14 and 21 days, at each time point, the cells were fixed in 75% ethanol for 1 h, followed by staining with 2% Alizarin Red solution for 10 min. Afterwards, the celladhered plates were washed with distilled water until color absence. The staining images of ECM mineralization were captured at day 21 of incubation. For quantitative analysis, the stain on the culture plate that BMSCs were cultured for 14 and 21 days with CCM was dissolved in 10 mM $\rm Na_3PO_4$ solution containing 10 vol% cetylpyridinum chloride, and the absorbance values were measured at 620 nm. Three replicated wells were set up for each type of CCM at each incubation time to run the tests, and the tests were independently performed four times.

2.6. Animal experiments

2.6.1. Animals and surgery

All the animal experiments were conducted according to the ISO 10993-2: 2006 animal welfare requirements, and all the procedures in the animal experiments were approved by the animal research committee of Xi'an Jiaotong University. Eighteen adult rats (about 250 g) were employed to evaluate the osseointegration of 0FMSN- and 20FMSN-coated Mg and bare Mg pillars (six for each group), and the bare Mg pillar was defined as the control group. The rats were anesthetized by an intramuscular injection of 2.5 wt% pentobarbital sodium solution. Two holes (Φ 1.6 mm) were respectively drilled in the right and left femoral condyles of each rat; then, the pillars were inserted, followed by suturing the muscle, subcutaneous tissue, and skin. Postoperatively, the rats were received brizolina intramuscular injection for three days and allowed to move freely in cages.

2.6.2. Histological examinations assays

After 4 weeks of surgery, the rats were sacrificed. The femora containing the implanted pillars (n = 6 for each group) were fixed in formalin, dehydrated by ethanol with ascending concentrations, and polymethyl methacrylate (PMMA) were used for embedding. The embedded samples were cut into sections (~150 μm thickness) using a microtome (Leitz 1600, Germany); the sections were ground, polished to foils with a thickness of 20 μm , and subsequently stained with Van Gieson's picric–fuchsine for histological analysis. The sections were observed by an Olympus IX 71 microscope (USA) and analyzed using Image-Pro Plus software.

2.6.3. Micro-CT assay

Micro-CT assay was used to evaluate the remaining volumes of the coated and bare Mg pillars and peri-implant bone formation after 4 weeks of implantation in the femoral condyles of rats. The rats implanted with the pillars were sacrificed followed by collecting the femora containing the pillars and scanning by a Micro-CT device (ALOKA, Hitachi, Japan) for 3D reconstruction with an image resolution of 8 µm. The 3D high-resolution reconstructed images were obtained and analyzed with the software of mimics 10.01 (Materialise, Belgium).

2.7. Statistical analysis

The data were expressed as mean \pm standard deviation (SD) from repeated independent experiments. The data were analyzed using SPSS 16.0 software (USA). A one-way ANOVA followed by a least-significant-difference (LSD) post hoc test was used to determine the level of

significance. Here, p < 0.05 and 0.01 were considered to be significant and highly significant, respectively.

3. Results

3.1. Microstructures of the coatings

The morphologies, phase identification and chemical species of the synthesized MSNs before and after F grafting were shown in Fig. S1, revealing the successful F^- encapsulation but without destroying the mesoporous structure of MSNs.

Fig. 2 shows the microstructural features of the different layers formed on Mg. The MAOed layer (i.e. MAOo coating) displayed a porous morphology with 2 ~ 3 µm diametric pores homogeneously distributing over its surface (Fig. 2A1), and the layer composed of MgO as identified by XRD in Fig. 2B. After spin-coating treatment, the microspores in the MAOed layer were sealed with the PLA, which further formed an integrate layer to overlay the MAOed layer (Fig. 2A2). The PLA layer exhibited a macroscopic wrinkled morphology, but each of the microcosmic winkles was smooth (inset in Fig. 2A2). However, after mixing cFMSNs into the PLA solution, some granules were observed in the winkles of the cFMSNs@PLA layer (as marked by arrows in Fig. 2A3), which were the agglomeration of the cFMSNs as confirmed by the XRD pattern in Fig. 2B. In addition, with increasing the loading amounts of cFMSNs, more granules were observed in the cFMSNs@PLA layer, and the original macroscopic wrinkled morphologies became more flat and compact (Fig. 2A4 and A5). After Ca-P depositing, platelike crystals composed of DCPD, as confirmed by XRD (Fig. 2B), were formed above the spin-coating derived layer. The cross-sectional morphology of 20FMSN, as a representative, was shown in Fig. 2C. With the aid of EDX profiles of Ca, P, O and Mg on the cross-section of the coating, it was clearly drawn that the coating comprised three-layered structure with DCPD as an outer layer, cFMSNs@PLA as an interlayer and cFMSNs@PLA sealed MgO as an inner layer adjacent to Mg. Notably, no discontinuities were observed at the interlaminar interfaces and the coating/substrate interface, revealing the firm adhesion within the interlayers and between the coating and Mg substrate.

3.2. Self-healing, corrosion resistance and drug release properties of the coatings

LEIS assay was carried out to investigate the local corrosion resistance of the artificial defect-contained coatings after 24 h of immersion in PS. To observably demonstrate the descending amplitude of the impedance values, the percentages between the impedance values respectively obtained from the inside and outside areas of the artificial defects contained in the coatings were shown in LEIS 3-dimensional maps (Fig. 3A). The impedance value within the artificial defect in 0FMSN displayed the most pronounced decline amplitude of about 67.23%, and the decline percentages of the impedance values within artificial defects in 5FMSN, 10FMSN, and 20FMSN coatings were about 39.02%, 27.06% and 23.96%, respectively. The results revealed that the coatings with cFMSNs exhibited self-healing capability to maintain higher corrosion resistance even though the appearance of the defects during immersion. In addition, the self-healing capability of the coatings was enhanced with increasing the loading amounts of cFMSNs.

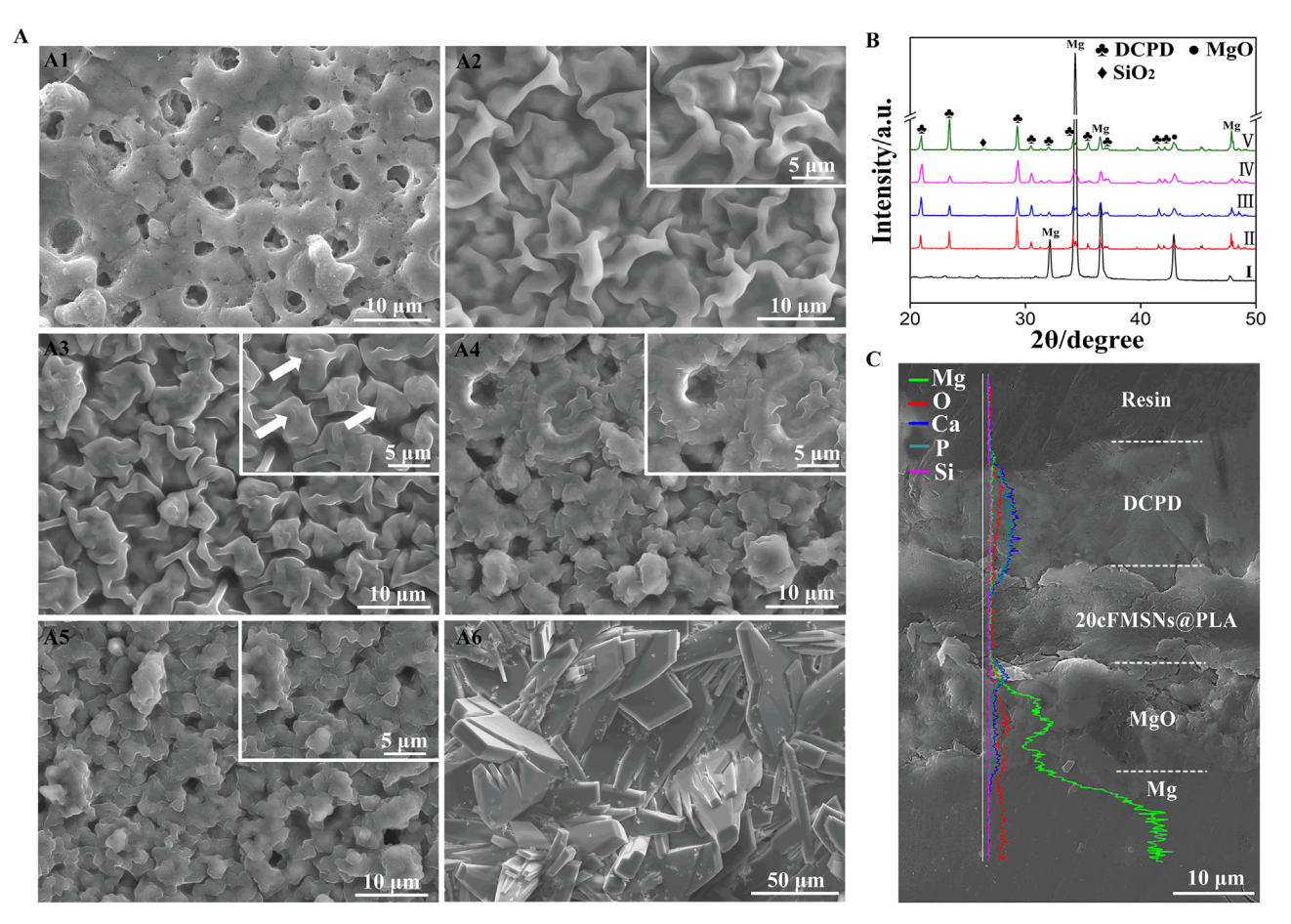


Fig. 2. (A) Surface morphologies of (A1) MAO₀, (A2) PLA layer without cFMSNs spin coated on the MAOed layer, (A3) 5 wt% cFMSNs contained-PLA layer spin coated on the MAOed layer (5cFMSNs@PLA/MgO), (A4) 10 wt% cFMSNs contained-PLA layer spin coated on the MAOed layer (10cFMSNs@PLA/MgO), (A5) 20 wt % cFMSNs contained-PLA layer spin coated on the MAOed layer (20cFMSNs@PLA/MgO), (A6) the chemical deposited DCPD layer on 20cFMSNs@PLA/MgO; (B) XRD spectra of (I) MAO₀, (II) 0FMSN, (III) 5FMSN, (IV) 10FMSN and (V) 20FMSN; (C) the cross-sectional morphology of 20FMSN.

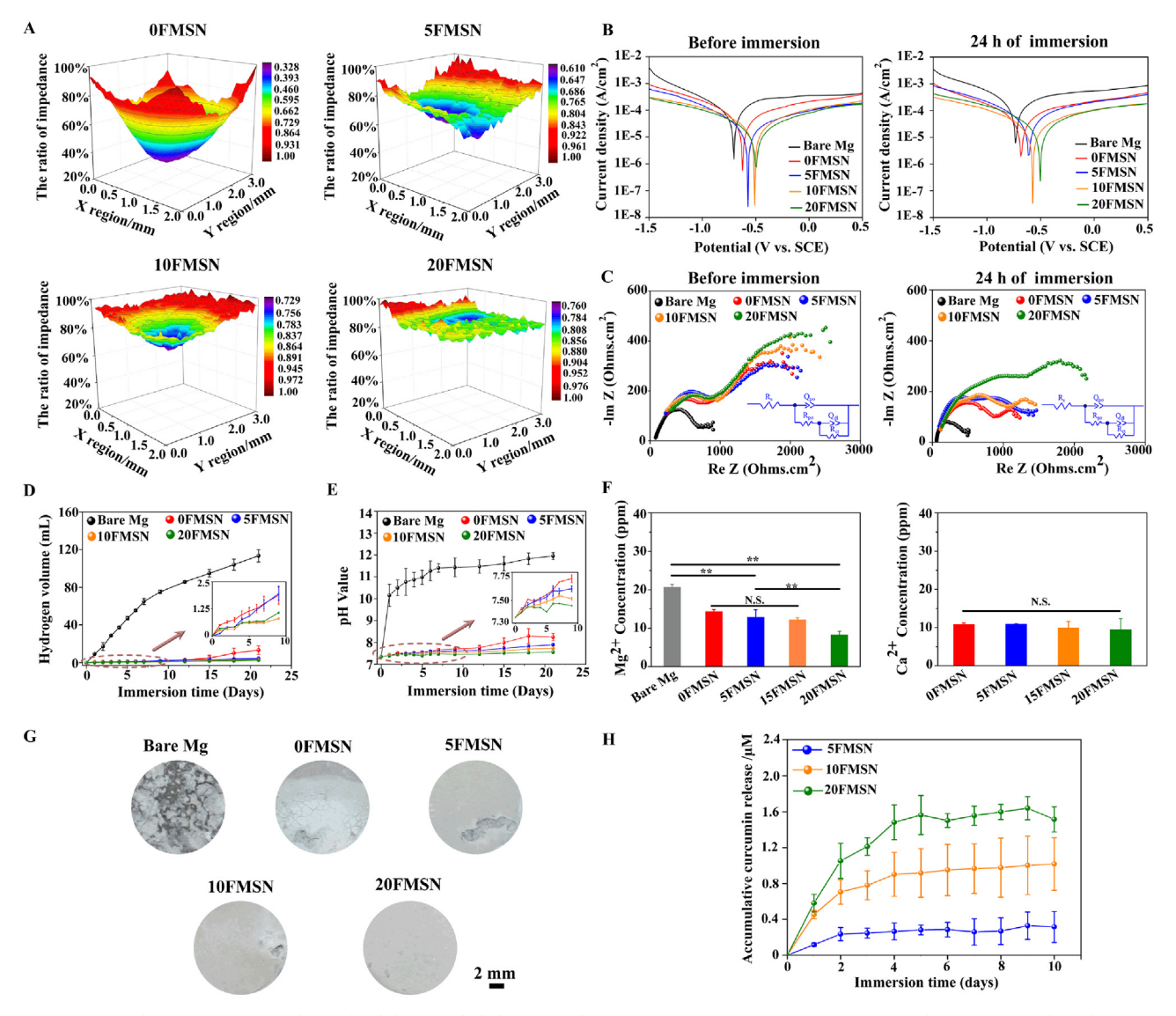


Fig. 3. (A) LEIS impedance mapping over the artificial defect included areas on the surfaces of 0FMSN-, 5FMSN-, 10FMSN-, and 20FMSN-coated Mg discs after 24 h of immersion in PS solutions; (B) polarization curves and (C) Nyquist plots of EIS spectra of the bare and coated Mg discs before and after 24 h of immersion in PS solutions, and the insets showing the equivalent circuits used to fit the impedance data of the bare and coated Mg discs; (D) hydrogen volumes released by the bare and coated Mg discs immersed in the PS solutions and (E) pH values of the PS solutions immersing the bare and coated Mg discs as a function of time; (F) Mg^{2^+} and Ca^{2^+} concentrations of the PS solutions; (H) the curves of the accumulative released curcumin concentrations measured in the PS solutions immersing the 5FMSN-, 10FMSN-, and 20FMSN-coated Mg discs as a function of immersion time. N.S.: no significance, (*) p < 0.05, (**) p < 0.01.

Table 1
Corrosion potentials (E_{corr} values) and corrosion current densities (i_{corr} values) obtained from the polarization curves of the bare, 0FMSN, 5FMSN, 10FMSN, 20FMSN-coated Mg discs and EIS fitted parameters of the equivalent circuits for the bare, 0FMSN, 5FMSN, 10FMSN and 20FMSN-coated Mg discs before and after 24 h of immersion in PS solutions.

Samples	Before immersion						24 h of immersion			
	Bare Mg	0FMSN	5FMSN	10FMSN	20FMSN	Bare Mg	0FMSN	5FMSN	10FMSN	20FMSN
E _{corr} (V. vs SCE)	-0.70	-0.62	-0.57	-0.51	-0.50	-0.73	-0.68	-0.61	- 0.57	-0.50
i _{corr} (μA/cm ²)	74.13	30.90	13.18	12.02	12.30	165.96	38.02	25.07	14.13	12.88
$R_s(\Omega)$	65.86	42.66	60.7	51.56	48.70	52.2	47.57	48.44	39.64	51.80
$R_{po} (\Omega \cdot cm^2)$	691.8	925.2	999.6	1024	1395	183.6	852.2	972.7	1019	1083
Q _{po} (μF·cm ⁻²)	65.05	15.46	11.12	10.49	49.22	641.20	1276	163.2	1180	36.43
n _{po}	0.51	0.80	0.44	0.51	0.51	0.8	0.51	0.39	0.44	0.38
$R_{ct} (\Omega \cdot cm^2)$	135	1626	1642	1759	1970	292.7	462.4	484.9	764.9	1699
$Q_{dl} (\mu F \cdot cm^{-2})$	3123	334.5	390.9	287.9	294.8	10.05	24.31	163.2	29.66	19.18
n _{dl}	0.85	0.8	0.45	0.44	0.30	0.80	0.46	0.67	0.44	0.46

To further investigate the protective efficacy and confirm the self-healing capability of the coatings after long term immersion, electrochemical and immersion tests were carried out. Fig. 3B shows the PDP curves of the bare and coated Mg discs before and after 24 h of immersion in PS, from which the corrosion potentials (Ecorr) and corrosion current densities (icorr) of the samples could be drawn as summarized in Table 1. Before immersion, the 5FMSN-, 10FMSN-, and 20FMSN-coated Mg discs exhibited similar icorr, which were lower than the 0FMSN-coated Mg disc, and much lower than the bare Mg. In addition, Mg with the cFMSNs contained coatings showed more positive Ecorr compared to the 0FMSN-coated Mg and bare Mg discs. After 24 h of immersion, the icorr of all the samples increased but with different amplitudes, following the trend of bare Mg $\,>\,$ 0FMSN $\,\approx\,$ 5FMSN $\,>\,$ 10FMSN $\,>\,$ 20FMSN.

Fig. 3C exhibits the Nyquist plots drawn from EIS spectra of the bare and coated Mg discs before and after 24 h of immersion in PS. All the samples exhibited similar features with two capacitance loops before and after immersion: the high-frequency one was attributed to the corrosive solution penetrating into the fabricated coatings or the corrosion-derived layer (for bare Mg) [40], and the lower one was associated with Faradaic charge transfer reactions at the interfaces of the coatings/corrosion-derived layer and Mg substrates [41–43]. The equivalent circuits (ECs) used to fit the impedance data of the samples were shown in the insets of Fig. 3C. In the ECs, $R_{\rm s}$ is the resistance of PS solution; $Q_{\rm dl}$ and $R_{\rm ct}$ represent the capacitance of electric double layer and charge transfer resistance at coating/substrate interface; $Q_{\rm po}$ and $R_{\rm po}$ are the capacitance and solution penetration resistance. The fitted parameters of the ECs were presented in Table 1. Before immersion, all the coated Mg discs showed larger $R_{\rm po}$ and $R_{\rm ct}$ values than bare Mg,

suggesting the coatings could effectively impair the penetration of corrosive solution to react with Mg substrates. The protective efficacy was enhanced with increasing the cFMSNs loading amounts, ascribing to the gradually increased compactness of the cFMSNs@PLA interlayers in the cFMSNs contained coatings (Fig. 2A3-5). After 24 h of immersion, the $R_{\rm po}$ and $R_{\rm ct}$ values of all the coated Mg discs decreased, while the decline amplitudes of the $R_{\rm po}$ and $R_{\rm ct}$ values, especially the $R_{\rm ct}$ values, were quite different. The 0FMSN-, 5FMSN-, 10FMSN- and 20FMSN-coated Mg discs exhibited 71.56%, 70.47%, 56.52% and 13.76% decreases in $R_{\rm ct}$ values, respectively, revealing the still more effective protection of 20FMSN to Mg substrate after immersion. The electrochemical test results revealed that increasing the cFMSNs loading amounts endowed the coatings with improved self-healing capability to enhance the protective effects to Mg substrates against corrosion during immersion

The hydrogen evolution and alkalization of the solution immersing the bare and coated Mg discs were monitored and displayed in Fig. 3D and E. During the immersion period, the amounts of released H_2 from all the samples increased but with different increments. At each time point, the bare Mg disc released the largest amount of H_2 among all the samples, indicating its fast corrosion. However, the coated Mg discs significantly decreased H_2 production compared to the bare Mg disc, and the decrements were more pronounced for the Mg discs with cFMSNs contained coatings, especially for the 20FMSN-coated Mg disc after long term immersion. pH value was another indicator of Mg corrosion. The alkalization of the coated Mg discs immersed solutions were lowered compared to that of the bare Mg disc immersed solution within the whole duration of immersion, of which, the 20FMSN-coated Mg disc induced the slightest alkalization of its surrounding solution. Besides H_2

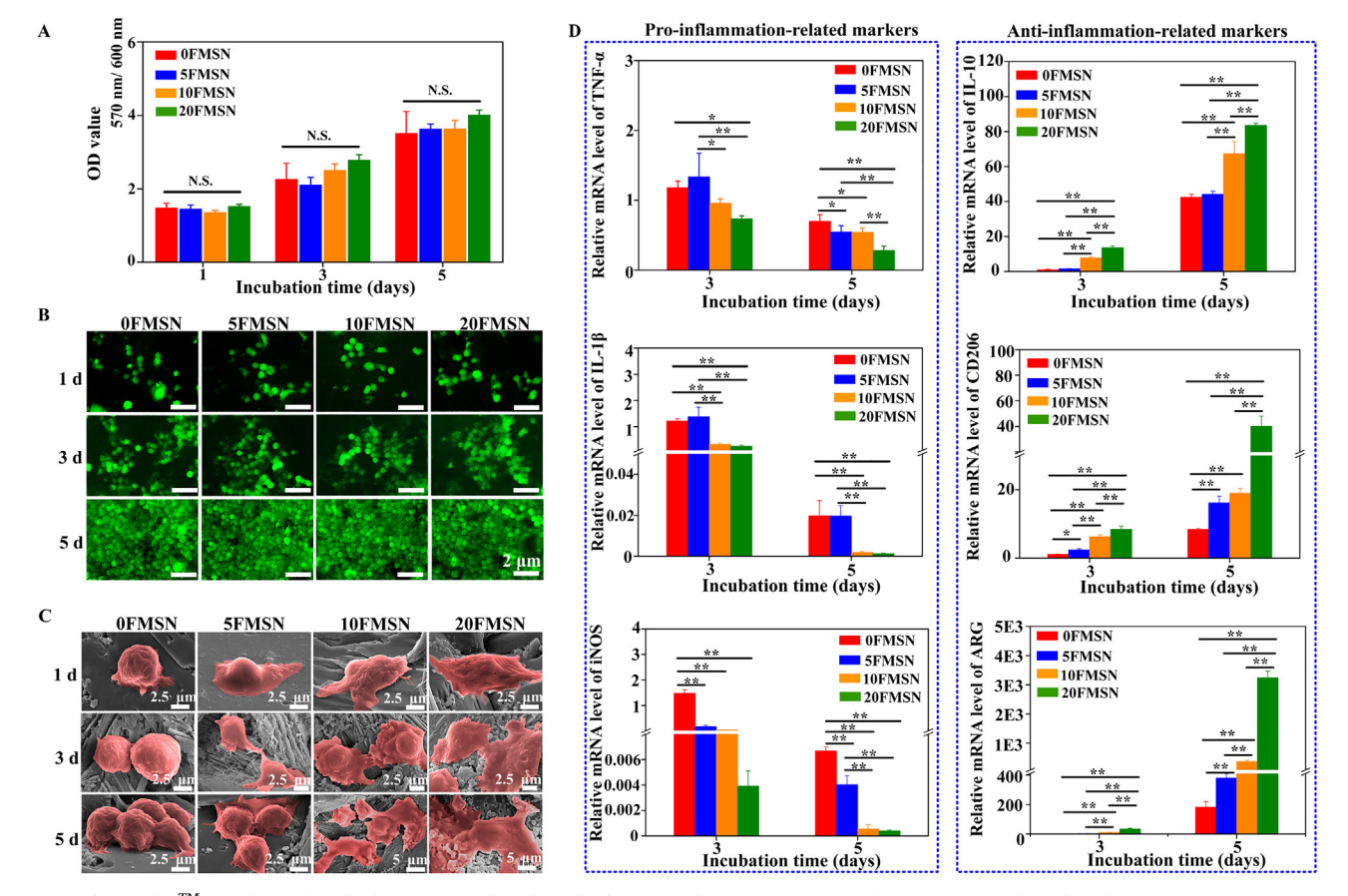


Fig. 4. (A) AlamarBlueTM tested mitochondrial activities and (B) live/dead staining fluorescent images of the RAW264.7 cultured on the 0FMSN-, 5FMSN-, 10FMSN-, and 20FMSN-coated Mg discs for 1, 3 and 5 days; (C) FE-SEM images of the RAW264.7 cultured on the coated Mg discs for 1, 3 and 5 days; (D) gene expressions of the RAW264.7 cultured on the coated Mg discs for 3 and 5 days; pro-inflammatory cytokines TNF- α , IL-1 β , iNOS and anti-inflammatory cytokines IL-10, CD206, ARG. Data are presented as mean \pm SD, n = 4, N.S.: no significance, (*) p < 0.05, (**) p < 0.01.

evolution and alkalization of the solutions, the degradation of MgO layers in the coatings and underlying Mg altered the Mg²⁺ concentrations of the solutions immersing the coated and bare Mg discs; in parallel, the degradation of the DCPD layers in the coatings released Ca²⁺ into their surrounding solutions. After 3 days of immersion, the Mg²⁺ concentrations of the PS immersing the bare and coated Mg discs and Ca²⁺ concentrations of the PS immersing the coated Mg discs were shown in Fig. 3F. The coated Mg discs resulted in lower Mg2+ concentrations of their surrounding solutions compared to the bare Mg. Notably, the 0FMSN-, 5FMSN- and 10FMSN-coated Mg discs induced about 14 ppm Mg²⁺, while much lower amount of Mg²⁺ (8.26 ppm) was detected in the 20FMSN-coated Mg disc immersed solution, indicating more effective inhibition of Mg and MgO degradation by 20FMSN. However, the Ca²⁺ concentrations of the PS immersing the coated Mg discs were comparable due to the similar degradation rates of the outer DCPD layers in the coatings.

The macroscopic corrosive morphologies of the bare and coated Mg discs after 21 days of immersion in PS were shown in Fig. 3G. The whole surface of the bare Mg disc was corroded to form large amounts of corrosion pits and cracks with corrosion products deposition, while fewer of cracks and corrosion pits were observed on the coated Mg discs, and the amounts of cracks and corrosion pits became less pronounced with increasing cFMSNs loading amounts in the coatings.

The curcumin release behaviors of the cFMSNs contained coatings were tested, as shown in Fig. 3H. The release curves of all the coatings showed similar features, exhibiting the burst release within 4 days of immersion but with different amounts. It showed that the accumulative curcumin concentrations of the PS immersing 5FMSN, 10FMSN and 20FMSN for 4 days was about 0.26, 0.90 and 1.48 μM . After that, the curcumin release from each kind of the coated Mg discs reached a

plateau range and at day 10, the accumulative concentrations of released curcumin were about 0.31, 1.02 and 1.51 μM for 5FMSN, 10FMSN and 20FMSN, respectively. The curcumin release rates from the coated Mg discs were lower than those from curcumin-loaded MSNs and curcumin-loaded PCL-poly ethylene glycol (PEG) coating [29,44], which may attribute to the blocking effects of the PLA and the outer layer of DCPD as well as the controllable release effects of FMSNs.

3.3. Cytocompatibility, osteoimmunomodulation and osteogenesis of the coatings

AlamarblueTM assay and live/dead fluorescent staining of macrophages cultured on the coated Mg discs were performed after 1, 3 and 5 days of incubation, as shown in Fig. 4A. The mitochondrial activities and the live cell numbers of macrophages cultured on the coated Mg discs increased with incubation time but without significant differences between the groups, indicating the good cytocompatibilities of all the coatings. The morphology variations of the macrophages cultured on the coated Mg discs for 1, 3 and 5 days were examined by FE-SEM. The macrophages cultured on the 0FMSN-coated Mg disc exhibited spherical shape and spread less during the incubation period. However, the cells spread out on the Mg discs with cFMSNs contained coatings, especially on the 20FMSN-coated Mg disc, growing into large sized polygonal cells with prolonging incubation time.

The changes in macrophage morphology has been demonstrated to be associated with its phenotype. It has been reported that polarized M1 macrophage exhibited a round-like shape without spread, while the M2 macrophages displayed spindle-shaped and better spreading morphology [45,46], suggesting that the macrophages cultured on the cFMSNs-contained coatings (especially on 20FMSN) were polarized into

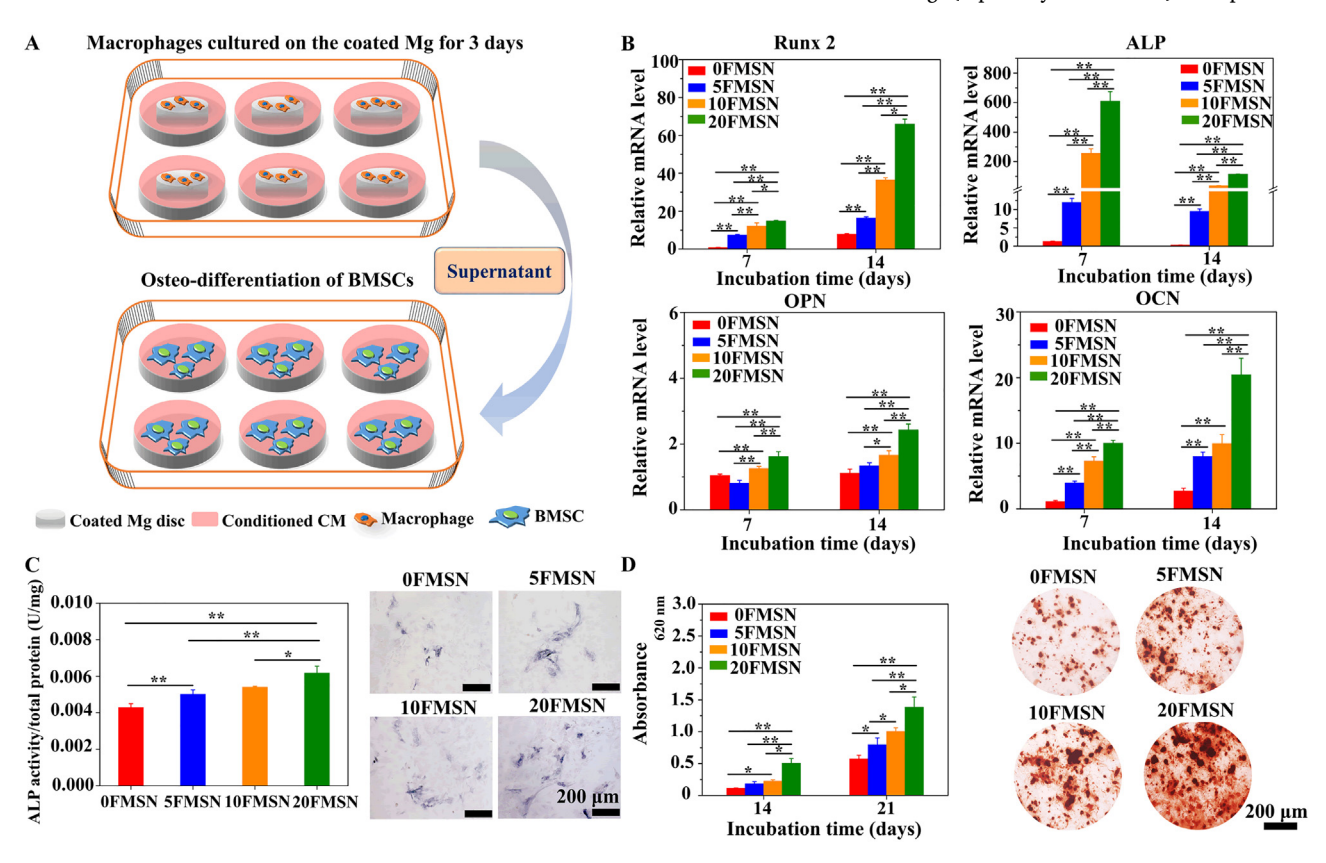


Fig. 5. (A) Schematic diagram showing the procedure of extracting macrophages-conditional culture medium (CCM) to culture the BMSCs seeded on tissue culture plates; (B) gene expressions of osteogenic markers Runx2, ALP, OPN and OCN of the BMSCs cultured with CCM for 7 and 14 days; (C) ALP activities and ALP staining pictures of the BMSCs cultured with CCM for 7 days; (D) alizarin red staining assessed quantitative values of the BMSCs cultured with CCM for 14 and 21 days and the staining pictures taken at day 21 as a visual example. Data are presented as the mean \pm SD, n=4, (*) p<0.05 and (**) p<0.01. (For interpretation of the references to color in this figure legend, the reader is referred to the web version of this article.)

M2 phenotype at an earlier time than those cultured on 0FMSN. To further clarify the modulation effects of the coated Mg discs on the phenotypes of macrophage, the pro-inflammation-related (M1) and anti-inflammation-related (M2) genes of macrophages cultured on the coatings for 3 and 5 days were evaluated, as shown in Fig. 4D. For each kind of the coatings, the macrophage-secreted pro-inflammatory cytokines, TNF-α, IL-1β and iNOS were downregulated, while the anti-inflammatory cytokines, IL-10, CD206 and ARG were upregulated over time, indicating the beneficial anti-inflammatory effects of all the coatings. However, at each incubation time point, the TNF- α , IL-1 β and iNOS were significantly downregulated by the cFMSNs contained coatings compared to 0FMSN, and the decline was most pronounced for the cells cultured on 20FMSN: simultaneously, IL-10, ARG and CD206 genes were highly upregulated by the cFMSNs contained coatings, especially for the coatings loaded with more amount of cFMSNs. The results indicated that the Mg discs with cFMSNs contained coatings quickly switched the phenotype of macrophages from M1 to M2 compared to the OFMSN-coated Mg disc and shortened the lasting duration of inflammation, of which, the coatings containing higher amounts of cFMSNs showed more efficient modulation.

It has been reported that the cytokines secreted by the M1 and M2 macrophages would induce significant different behaviors of osteogenic

cells [24,26]. In addition, Mg-based implants degradation derived alkalization of the culture medium, H₂ and ions release, such as Mg²⁺, could also impact the functions of osteogenic cells [6,47]. To determine the modulation effects of the macrophages-secreted cytokines and the coated Mg degradation derived alteration of the microenvironment on the osteo-differentiation of BMSCs, CCM were used to culture BMSCs seeded on tissue culture plate (TCP) for different time. CCM was the collected supernatant of the culture medium after culturing macrophages seeded on the coated Mg discs for 3 days, as schematically illustrated in Fig. 5A and termed as M/0FMSN CCM, M/5FMSN CCM, M/ 10FMSN CCM and M/20FMSN CCM, respectively. Expressions of osteogenesis-related genes, including Runx2, ALP, OPN and OCN of the BMSCs cultured with CCM on TCP for 7 and 14 days were detected, as shown in Fig. 5B. The mRNA expressions of Runx2, OPN and OCN in the BMSCs cultured with all the CCM increased with incubation time from 7 to 14 days, while the ALP mRNA expressions at day 14 were obviously down-regulated compared to those in the cells cultured in the corresponding CCM at day 7, attributing to the beginning mineralization of BMSCs [47]. It is worth noticing that at each time point, M/ 5FMSN CCM, M/10FMSN CCM and M/20FMSN CCM significantly upregulated the Runx2, OPN, OCN and ALP gene expressions of the BMSCs compared to M/0FMSN CCM but with different increments,

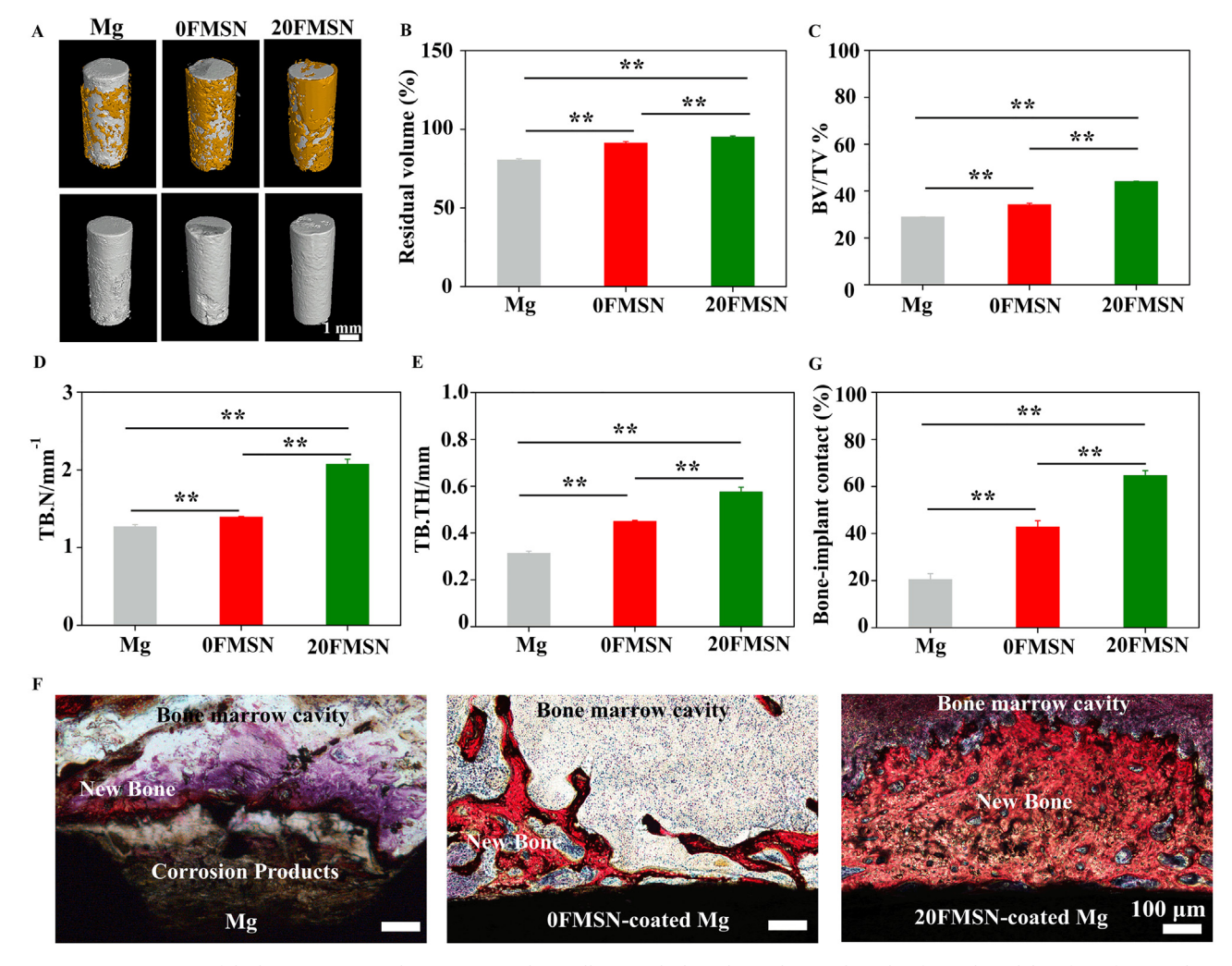


Fig. 6. (A) Micro-CT images of the bare, 0FMSN-, and 20FMSN-coated Mg pillars (marked in white color) implanted in femoral condyles of rats for 4 weeks with or without the *peri*-implant bone (marked in yellow color) and (B) residual volumes of the pillars; quantitative analysis of (C) bone volume fraction (BV/TV), (D) trabecular number (TB. N), (E) trabecular thickness (TB. TH) of the *peri*-implant bone calculated from the Micro-CT assay; (F) histological stained images at implantation time of 4 weeks of the bare, 0FMSN-, and 20FMSN-coated Mg pillars; and (G) corresponding bone-implant contacts. Data are presented as the mean \pm SD, n = 6, (*) p < 0.05 and (**) p < 0.01. (For interpretation of the references to color in this figure legend, the reader is referred to the web version of this article.)

following the order of M/5FMSN CCM < M/10FMSN CCM < M/ 20FMSN CCM. Fig. 5C showed the quantified ALP activities and ALP staining assay of the BMSCs cultured with CCM for 7 days. The variation trends of the ALP activities and its expressions at protein level in BMSCs were similar with that of the gene expression at day 7 (Fig. 5B), indicating that the ALP synthesis in BMSCs was significantly enhanced by the cFMSN contained-coatings resultant CCM, especially for M/ 20FMSN CCM. Fig. 5D shows the Alizarin red staining assays of ECM mineralization of the BMSCs cultured with CCM for 14 and 21 days. The results revealed that the cFMSNs contained-coatings resultant CCM significantly enhanced ECM mineralization of BMSCs comparted to M/ 0FMSN CCM, and the enhancement followed the trend of M/5FMSN CCM < M/10FMSN CCM < M/20FMSN CCM. These results indicated that the cFMSNs contained-coatings resultant CCM accelerated BMSCs osteo-differentiation by means of promoting cells to a mature phenotype and expediting ECM mineralization, and more cFMSNs containedcoatings resultant CCM exhibited more pronounced enhancement.

Fig. 6A shows the micro-CT images, reconstructed with and without the new bone, of the bare and coated Mg pillars implanted in femoral condyles of rats for 4 weeks. The bare Mg pillar underwent the most pronounced volume reduction, but the volume reduction was slight for the coated Mg pillars, especially for the 20FMSN-coated Mg pillar, showing almost no volume reduction after 4 weeks of implantation (Fig. 6A and B). The results revealed the effective protection of the cFMSN contained coatings to Mg substrates, keeping in line with the results of the corrosion tests in vitro (Fig. 3). Furthermore, the reconstructed Micro-CT images exhibited that the 20FMSN-coated Mg pillar induced more new bone formation than the 0FMSN-coated Mg pillar and far more than the bare Mg pillar (Fig. 6A), which was further proved by the quantitative results shown in Fig. 6C. In parallel, the quantitative analysis results in Fig. 6D and E also identified that both the trabecular thicknesses and trabecular numbers within the peri-implant new bone followed the order of 20FMSN > 0FMSN > bare Mg. These results revealed that the quantity and quality of the newly formed bone around the 20FMSN-coated Mg pillar were higher than those of new bone around the OFMSN-coated Mg pillar and much higher than those of new bone around the bare Mg pillar. The aforementioned results were also supported by the histological stained images, as shown in Fig. 6F, from which the bone-implant contact ratios could be assessed (Fig. 6G). The 20FMSN-coated Mg pillar showed the highest bone-implant contact ratio, followed by the 0FMSN-coated Mg pillar, and then the bare Mg pillar with the lowest contact ratio.

4. Discussion

To inhibit the severer pitting corrosion and keep long-term mechanical integrity of Mg-based endosseous implants, construction of a self-healing coating on Mg is a novel strategy. In the present work, FMSNs were employed as CIs and loaded in the coating, which could release F to react with the degradation-derived Mg2+ to form precipitation film for sealing micro-defects in the coating that originated from the corrosive fluids penetration during implantation [19,39]. Therefore, the cFMSNs contained coatings exhibited effective long term protection to Mg substrates to inhibit large amount of H2 evolution, Mg²⁺ release and alkalization of their surrounding solutions (Fig. 3D-G). Moreover, increasing the cFMSNs loading amounts in the coatings would further impair the corrosion pits formation on Mg substrates (Figs. 3G and 6A), keeping longer term mechanical integrity [6,7]. On one hand, with increasing the cFMSNs loading amounts, the interlayers in the coatings became more compact to effectively impair the penetration of corrosive fluids (Figs. 2A, 3B and C), on the other hand, more cFMSNs significantly enhance the self-healing capability of the coating (Fig. 3A). Notably, different from other CIs, such as Ce²⁺ [15], the precipitation layer induced by F⁻ and Mg²⁺ (i.e. MgF₂) could be gradually degraded by the Cl - contained body fluids, decreasing the risk of osteolysis induced by the debris of insoluble passive film [20].

In addition, FMSNs could also be used as nanovehicles to controllably release curcumin for modulating the macrophages-mediated inflammatory response (i.e. osteoimmunomodulation), which plays a key role in osseointegration of endosseous implants. Actually, the quick switch of the macrophages from M1 to M2 phenotype at initial implantation stage promotes the recruitment of BMSCs on implants and subsequent osteo-differentiation [24,26]. Curcumin could inhibit M1 macrophage phenotype by blocking nuclear factor kappa-light-chainenhancer of activated B cells (NF-kB) expression and induce M2 phenotype through the activation of proliferator-activated receptor gamma (PPAR-γ) pathway with a dose dependent manner [48,49]. It has been reported that within 0.5 uM, higher concentration of curcumin in the culture medium would be beneficial for switching the phenotype of macrophages to M2 [32]. As highlighted in Fig. 3H, the loaded curcumin in the coated Mg discs was continuously released with an initial burst release followed by steady release manner, and curcumin concentrations of the PS immersing 5FMSN, 10FMSN and 20FMSN rose to $0.31~\mu M,~1.02~\mu M$ and $1.51~\mu M$ after 10 days of release. Although the accumulative release amount from 10FMSN and 20FMSN were higher than 0.5 µM, as calculated according to Fig. 3H and based on the experiment procedure of refreshing the culture medium of macrophages every two days, the curcumin concentrations of the culture medium surrounding 5FMSN-, 10FMSN-, and 20FMSN-coated Mg at day 3 were about 0.01 μ M, 0.075 μ M and 0.16 μ M, respectively. Therefore, all the cFMSNs contained coatings induced a quick M1 to M2 phenotype switch of the macrophages within 3 days, and 20FMSN exhibited the most effective osteoimmunomodulation towards anti-inflammation (Fig. 4D).

Progressively, the cFMSNs-contained coatings accelerated the osteodifferentiation and ECM mineralization of BMSCs as proved by the dramatically upregulated osteognesis-related markers both at gene and protein levels (Fig. 5B and C). Of which, 20FMSN-coated Mg exhibited the most pronounced promotion and thus the best osseointegration performance in vivo (Fig. 6). On one hand, the quick switch of immune microenvironment to anti-inflammation modulated by 20FMSN could facilitate the secretion of bone morphogenetic protein 2 (BMP2) of macrophages [50], which would bind to the BMP receptor type-2 (BMPR2), leading to the activation of mothers against decapentaplegic homologue 5 (SMAD5). The activated SMAD5 could form a complex with SMAD4, which translocated into the nucleus, facilitating the expression of distalless homeobox5 (Dlx5). The Dlx5 induced the expression of Runx2, resulting in osteo-differentiation of BMSCs to accelerate bone healing [36,51]. On the other hand, the degradationderived ions released from the cFMSNs-contained coatings, such as Mg²⁺ and Ca²⁺, would also contribute to osseointegration. It has been reported that controllable delivery of Mg²⁺ (within 200 ppm) elevated proliferation and osteo-differentiation of osteoblasts, and the enhancement was more obvious with increasing Mg²⁺ concentrations [52]; Ca²⁺ in cell culture medium would upregulate the intracellular Ca2+ concentrations [53,54] to enhance the proliferation and osteodifferentiation of osteogenic cells [55]. In addition, it has been reported that moderate amounts of H2 led to the obviously higher ALP activity of pre-osteoblasts [56] and increasing pH of the culture medium to 8-8.5 enhanced the proliferation and ALP activity of osteoblasts [57]. However, in our present work, 20FMSN-coated Mg with the best osseointegration performance (Figs. 5 and 6) induced the lowest Mg²⁺ concentration in its surrounding solution compared to 0FMSN-coated and bare Mg, and comparable Ca²⁺ concentration in the solution compared to 0FMSN-coated Mg (Fig. 3F). Moreover, within 3 days of immersion, the H₂ release from 20FMSN-coated Mg was similar with that of OFMSN-coated Mg, and the pH values of the solutions immersing 0FMSN- and 20FMSN-coated discs were also comparable and lower than 8 (insets in Fig. 3D and E). The results revealed that the enhanced osseointegration by 20FMSNs-coated Mg was mainly attributed to the osteoimmunomodulation capability of the coating.

5. Conclusions

A three-layered coating with self-healing function had been fabricated on Mg. The coating comprised an inner layer of MgO with FMSNs@PLA sealing the pores, an interlayer of FMSNs@PLA and an outer layer of plate-like DCPD, in which the FMSNs functioned as corrosion inhibitors. Furthermore, to endow the coating with immunomodulation capability, curcumin, as an immunomodulatory drug, was loaded in FMSNs (cFMSNs) to ensure its stable and controllable release. The cFMSNs contained coatings exhibited obvious self-healing effects to significantly inhibit the pitting corrosion formation on Mg substrates during 21 days of immersion in vitro and 4 weeks of implantation in vivo. Notably, the largest amount of cFMSNs contained coating (20FMSN) showed the most effective protection to Mg substrate against corrosion. Moreover, the cFMSNs contained coatings induced a quick phenotype switch of the macrophages from M1 to M2, significantly downregulated pro-inflammatory TNF-α, IL-1β, iNOS and upregulated anti-inflammatory IL-10, CD206, ARG, which was mainly attributed to the release of curcumin from the coatings. Consequently, 20FMSN with the highest release amount of curcumin modulated its surrounding immune microenvironment more efficiently towards antiinflammation to facilitate osteo-differentiation and ECM mineralization of BMSCs, achieving enhanced osseointegration by means of contact osteogenesis compared to the coatings with moderate (10FMSN) and lowest (5FMSN) release amounts of curcumin.

Declaration of Competing Interest

The authors declare that they have no known competing financial interests or personal relationships that could have appeared to influence the work reported in this paper.

Acknowledgements

We appreciate Research Fund for the National Natural Science Foundation of China (Grant number 51631007, 51971171 and 31700860), China Postdoctoral Science Foundation (2017M613128), Fundamental Research Funds for the Central Universities (xjj2018230), Natural Science Foundation of Shaanxi Province (2020JQ-052) and Key Research and Development Plan of Shaanxi Province (2018ZDXMGY119) for financially supporting this work.

Appendix A. Supplementary data

Supplementary data to this article can be found online at https://doi.org/10.1016/j.cej.2020.126323.

References

- [1] M.P. Staiger, A.M. Pietak, J. Huadmai, G. Dias, Magnesium and its alloys as orthopedic biomaterials: a review, Biomaterials 27 (2006) 1728–1734.
- [2] Y. Zheng, X. Gu, F. Witte, Biodegradable metals, Mater. Sci. Eng. R Rep. 77 (2014) 1–34.
- [3] G. Li, L. Zhang, L. Wang, G. Yuan, K. Dai, J. Pei, Y. Hao, Dual modulation of bone formation and resorption with zoledronic acid-loaded biodegradable magnesium alloy implants improves osteoporotic fracture healing: an in vitro and in vivo study, Acta Biomater. 65 (2018) 486–500.
- [4] Y. Guo, Y. Yu, L. Han, S. Ma, J. Zhao, H. Chen, Z. Yang, F. Zhang, Y. Xia, Y. Zhou, Biocompatibility and osteogenic activity of guided bone regeneration membrane based on chitosan-coated magnesium alloy, Mater. Sci. Eng. C 100 (2019) 226–235.
- [5] P. Xiong, Z. Jia, M. Li, W. Zhou, J. Yan, Y. Wu, Y. Cheng, Y. Zheng, Biomimetic Ca, Sr/P-Doped silk fibroin films on Mg-1Ca alloy with dramatic corrosion resistance and osteogenic activities, ACS Biomater. Sci. Eng. 4 (2018) 3163–3176.
- [6] B. Li, P. Gao, H. Zhang, Z. Guo, Y. Zheng, Y. Han, Osteoimmunomodulation, osseointegration, and in vivo mechanical integrity of pure Mg coated with HA nanorod/pore-sealed MgO bilayer, Biomater. Sci. 6 (2018) 3202–3218.
- [7] B. Li, Y. Han, K. Qi, Formation mechanism, degradation behavior, and cyto-compatibility of a nanorod-shaped HA and pore-sealed MgO bilayer coating on magnesium, ACS Appl. Mater. Interfaces 6 (2014) 18258–18274.
- [8] H. Duan, K. Du, C. Yan, F. Wang, Electrochemical corrosion behavior of composite

- coatings of sealed MAO film on magnesium alloy AZ91D, Electrochim. Acta 51 (2006) 2898-2908.
- [9] T.S. Narayanan, I.S. Park, M.H. Lee, Strategies to improve the corrosion resistance of microarc oxidation (MAO) coated magnesium alloys for degradable implants: prospects and challenges, Prog. Mater. Sci. 60 (2014) 1–71.
- [10] C. Ning, Z. Zhou, G. Tan, Y. Zhu, C. Mao, Electroactive polymers for tissue regeneration: developments and perspectives, Prog. Polym. Sci. 81 (2018) 144–162.
- [11] R.C. Zeng, L.Y. Cui, K. Jiang, R. Liu, B.D. Zhao, Y.F. Zheng, In vitro corrosion and cytocompatibility of a microarc oxidation coating and poly (I-lactic acid) composite coating on Mg–1Li–1Ca alloy for orthopedic implants, ACS Appl. Mater. Interfaces 8 (2016) 10014–10028.
- [12] L.Y. Li, L.Y. Cui, R.C. Zeng, S.Q. Li, X.B. Chen, Y. Zheng, M.B. Kannan, Advances in functionalized polymer coatings on biodegradable magnesium alloys-a review, Acta Biomater. 79 (2018) 23–26.
- [13] P. Tian, D. Xu, X. Liu, Mussel-inspired functionalization of PEO/PCL composite coating on a biodegradable AZ31 magnesium alloy, Colloids Surf. B: Biointerfaces 141 (2016) 327–337.
- [14] W. Wang, H. Wang, J. Zhao, X. Wang, C. Xiong, L. Song, R. Ding, P. Han, W. Li, Self-healing performance and corrosion resistance of graphene oxide-mesoporous silicon layer-nanosphere structure coating under marine alternating hydrostatic pressure, Chem. Eng. J. 361 (2019) 792–804.
- [15] Z. Jia, P. Xiong, Y. Shi, W. Zhou, Y. Cheng, Y. Zheng, T. Xi, S. Wei, Inhibitor encapsulated, self-healable and cytocompatible chitosan multilayer coating on biodegradable Mg alloy: a pH-responsive design, J. Mater. Chem. B 4 (2016) 2498–2511.
- [16] P. Xiong, J. Yan, P. Wang, Z. Jia, W. Zhou, W. Yuan, Y. Li, Y. Liu, Y. Cheng, D. Chen, A pH-sensitive self-healing coating for biodegradable magnesium implants, Acta Biomater. 98 (2019) 160–173.
- [17] A. Sugiyama, A. Mitsui, M. Okada, H. Yamawaki, Cathepsin S degrades arresten and canstatin in infarcted area after myocardial infarction in rats, J. Vet. Med. Sci. 81 (2019) 522–531.
- [18] J. Pajarinen, V.P. Kouri, E. Jämsen, T.F. Li, J. Mandelin, Y.T. Konttinen, The response of macrophages to titanium particles is determined by macrophage polarization, Acta Biomater. 9 (2013) 9229–9240.
- [19] Z.H. Xie, D. Li, Z. Skeete, A. Sharma, C.J. Zhong, Nanocontainer-enhanced self-healing for corrosion-resistant Ni coating on Mg alloy, ACS Appl. Mater. Interfaces 9 (2017) 36247–36260.
- [20] L. Mao, L. Shen, J. Chen, Y. Wu, M. Kwak, Y. Lu, Q. Xue, J. Pei, L. Zhang, G. Yuan, Enhanced bioactivity of Mg-Nd-Zn-Zr alloy achieved with nanoscale MgF₂ surface for vascular stent application, ACS Appl. Mater. Interfaces 7 (2015) 5320-5330.
- [21] R. Kotcherlakota, A.K. Barui, S. Prashar, M. Fajardo, D. Briones, A. Rodríguez-Diéguez, C.R. Patra, S. Gómez-Ruiz, Curcumin loaded mesoporous silica: an effective drug delivery system for cancer treatment, Biomater. Sci. 4 (2016) 448–459.
- [22] G. Chen, Z. Teng, X. Su, Y. Liu, G. Lu, Unique biological degradation behavior of Stöber mesoporous silica nanoparticles from their interiors to their exteriors, J. Biomed. Nanotechnol. 11 (2015) 722–729.
- [23] J.E. Davies, Bone bonding at natural and biomaterial surfaces, Biomaterials 28 (2007) 5058–5067
- [24] Q.L. Ma, L.Z. Zhao, R.R. Liu, B.Q. Jin, W. Song, Y. Wang, Y.S. Zhang, L.H. Chen, Y.M. Zhang, Improved implant osseointegration of a nanostructured titanium surface via mediation of macrophage polarization, Biomaterials 35 (2014) 9853–9867.
- [25] Y. Du, P. Ren, Q. Wang, S.K. Jiang, M. Zhang, J.Y. Li, L.L. Wang, D.W. Guan, Cannabinoid 2 receptor attenuates inflammation during skin wound healing by inhibiting M1 macrophages rather than activating M2 macrophages, J. Inflamm. 15 (2018) 1–12.
- [26] J.A. Jones, D.T. Chang, H. Meyerson, E. Colton, I.K. Kwon, T. Matsuda, J.M. Anderson, Proteomic analysis and quantification of cytokines and chemokines from biomaterial surface-adherent macrophages and foreign body giant cells, J. Biomed. Mater. Res. A 83 (2007) 585–596.
- [27] J. Chu, B. Yan, J. Zhang, L. Peng, X. Ao, Z. Zheng, T. Jiang, Z. Zhang, Casticin attenuates osteoarthritis-related cartilage degeneration by inhibiting the ROS-mediated NF- κ B signaling pathway in vitro and in vivo, Inflammation (2020) 1–11.
- [28] Z. Chen, T. Klein, R.Z. Murray, R. Crawford, J. Chang, C. Wu, Y. Xiao, Osteoimmunomodulation for the development of advanced bone biomaterials, Mater. Today 19 (2016) 304–321.
- [29] S. Bose, N. Sarkar, D. Banerjee, Effects of PCL, PEG and PLGA polymers on curcumin release from calcium phosphate matrix for in vitro and in vivo bone regeneration, Mater. Today Chem. 8 (2018) 110–120.
- [30] A.B. Kunnumakkara, D. Bordoloi, G. Padmavathi, J. Monisha, N.K. Roy, S. Prasad, B.B. Aggarwal, Curcumin, the golden nutraceutical: multitargeting for multiple chronic diseases, Br. J. Pharmacol. 174 (2017) 1325–1348.
- [31] R. Requejo Aguilar, A. Alastrue Agudo, M. Cases Villar, E. Lopez Mocholi, R. England, M.J. Vicent, V. Moreno Manzano, Combined polymer-curcumin conjugate and ependymal progenitor/stem cell treatment enhances spinal cord injury functional recovery, Biomaterials 113 (2017) 18–30.
- [32] Z. Yang, C. He, J. He, J. Chu, H. Liu, X. Deng, Curcumin-mediated bone marrow mesenchymal stem cell sheets create a favorable immune microenvironment for adult full-thickness cutaneous wound healing, Stem Cell Res. Ther. 9 (2018) 21.
- [33] S. Oh, T.W. Kyung, H.S. Choi, Curcumin inhibits osteoclastogenesis by decreasing receptor activator of nuclear factor-xB ligand (RANKL) in bone marrow stromal cells, Mol. Cells (Springer Science & Business Media BV) 26 (2008) 486–489.
- [34] N. Sarkar, S. Bose, Controlled delivery of curcumin and vitamin K2 from hydroxyapatite-coated titanium implant for enhanced in vitro chemoprevention, osteogenesis, and in vivo osseointegration, ACS Appl. Mater. Interfaces 12 (2020) 13644–13656.
- [35] Y. Xiong, B. Zhao, W. Zhang, L. Jia, Y. Zhang, X. Xu, Curcumin promotes osteogenic

- differentiation of periodontal ligament stem cells through the PI3K/AKT/Nrf2 signaling pathway, Iranian J. Basic Med. Sci. 23 (2020) 954–960.
- [36] Z. Chen, C. Wu, W. Gu, T. Klein, R. Crawford, Y. Xiao, Osteogenic differentiation of bone marrow MSCs by β-tricalcium phosphate stimulating macrophages via BMP2 signalling pathway, Biomaterials 35 (2014) 1507–1518.
- [37] J.E. Davies, V.C. Mendes, J.C. Ko, E. Ajami, Topographic scale-range synergy at the functional bone/implant interface, Biomaterials 35 (2014) 25–35.
- [38] L. Zhang, J. Pei, H. Wang, Y. Shi, J. Niu, F. Yuan, H. Huang, H. Zhang, G. Yuan, Facile preparation of poly (lactic acid)/brushite bilayer coating on biodegradable magnesium alloys with multiple functionalities for orthopedic application, ACS Appl. Mater. Interfaces 9 (2017) 9437–9448.
- [39] L.M. Calado, M.G. Taryba, M.J. Carmezim, M.F. Montemor, Self-healing ceria-modified coating for corrosion protection of AZ31 magnesium alloy, Corros. Sci. 142 (2018) 12–21.
- [40] Q. Yang, W. Yuan, X. Liu, Y. Zheng, Z. Cui, X. Yang, H. Pan, S. Wu, Atomic layer deposited ZrO2 nanofilm on Mg-Sr alloy for enhanced corrosion resistance and biocompatibility, Acta Biomater. 58 (2017) 515–526.
- [41] D. Song, A. Ma, J. Jiang, P. Lin, D. Yang, J. Fan, Corrosion behaviour of bulk ultrafine grained AZ91D magnesium alloy fabricated by equal-channel angular pressing, Corros. Sci. 53 (2011) 362–373.
- [42] G. Song, A. Atrens, D. St John, X. Wu, J. Nairn, The anodic dissolution of magnesium in chloride and sulphate solutions, Corros. Sci. 39 (1997) 1981–2004.
- [43] Y. Zhang, C. Yan, F. Wang, W. Li, Electrochemical behavior of anodized Mg alloy AZ91D in chloride containing aqueous solution, Corros. Sci. 47 (2005) 2816–2831.
- [44] C. Chen, W. Sun, X. Wang, Y. Wang, P. Wang, Rational design of curcumin loaded multifunctional mesoporous silica nanoparticles to enhance the cytotoxicity for targeted and controlled drug release, Mater. Sci. Eng. C 85 (2018) 88–96.
- [45] F.Y. McWhorter, T. Wang, P. Nguyen, T. Chung, W.F. Liu, Modulation of macrophage phenotype by cell shape, Proc. Nat. Acad. Sci. 110 (2013) 17253–17258.
- [46] X. Zheng, L. Xin, Y. Luo, H. Yang, X. Ye, Z. Mao, S. Zhang, L. Ma, C. Gao, Near-infrared-triggered dynamic surface topography for sequential modulation of macrophage phenotypes, ACS Appl. Mater. Interfaces 11 (2019) 43689–43697.
- [47] B. Li, Y. Han, M. Li, Enhanced osteoblast differentiation and osseointegration of a bio-inspired HA nanorod patterned pore-sealed MgO bilayer coating on magnesium,

- J. Mater. Chem. B 4 (2016) 683-693.
- [48] F. Chen, N. Guo, G. Cao, J. Zhou, Z. Yuan, Molecular analysis of curcumin-induced polarization of murine RAW264. 7 macrophages, J. Cardiovasc. Pharm. 63 (2014) 544–552.
- [49] T. Zhu, Z. Chen, G. Chen, D. Wang, S. Tang, H. Deng, J. Wang, S. Li, J. Lan, J. Tong, Curcumin attenuates asthmatic airway inflammation and mucus hypersecretion involving a PPARγ-dependent NF-κB signaling pathway in vivo and in vitro, Mediators Inflamm. 2019 (2019) 4927430.
- [50] C. Champagne, J. Takebe, S. Offenbacher, L. Cooper, Macrophage cell lines produce osteoinductive signals that include bone morphogenetic protein-2, Bone 30 (2002) 26–31.
- [51] C.S. Soltanoff, W. Chen, S. Yang, Y.P. Li, Signaling networks that control the lineage commitment and differentiation of bone cells, Crit. Rev. Eukar. Gene 19 (2009) 1–46.
- [52] Z. Lin, J. Wu, W. Qiao, Y. Zhao, K.H. Wong, P.K. Chu, L. Bian, S. Wu, Y. Zheng, K.M. Cheung, Precisely controlled delivery of magnesium ions thru sponge-like monodisperse PLGA/nano-MgO-alginate core-shell microsphere device to enable insitu bone regeneration, Biomaterials 174 (2018) 1–16.
- [53] L. Zhang, C. Yang, J. Li, Y. Zhu, X. Zhang, High extracellular magnesium inhibits mineralized matrix deposition and modulates intracellular calcium signaling in human bone marrow-derived mesenchymal stem cells, Biochem. Biophys. Res. Commun. 450 (2014) 1390–1395.
- [54] M.J. Berridge, M.D. Bootman, H.L. Roderick, Calcium: calcium signalling: dynamics, homeostasis and remodelling, Nat. Rev. Mol. Cell Biol. 4 (2003) 517–529.
- [55] M. Zayzafoon, Calcium/calmodulin signaling controls osteoblast growth and differentiation, J. Cell. Biochem. 97 (2006) 56–70.
- [56] H.M. Wong, Y. Zhao, V. Tam, S. Wu, P.K. Chu, Y. Zheng, M.K.T. To, F.K. Leung, K.D. Luk, K.M. Cheung, In vivo stimulation of bone formation by aluminum and oxygen plasma surface-modified magnesium implants, Biomaterials 34 (2013) 9863–9876.
- [57] Y. Shen, W. Liu, C. Wen, H. Pan, T. Wang, B.W. Darvell, W.W. Lu, W. Huang, Bone regeneration: importance of local pH—strontium-doped borosilicate scaffold, J. Mater. Chem. 22 (2012) 8662–8670.